Direct observation of the superallowed α decay of 104Te

Ian Cox

iancox02@gmail.com

University of Tennessee, Knoxville https://orcid.org/0000-0002-6807-3658

Robert Grzywacz

University of Tennessee, Knoxville

Thomas King

Oak Ridge National Laboratory

Krzysztof Rykaczewski

Oak Ridge National Laboratory https://orcid.org/0000-0002-5717-3418

Shunji Nishimura

RIKEN

Rin Yokoyama

University of Tokyo, Center for Nuclear Study

Naoki Fukuda

RIKEN

Noritaka Kitamura

The University of Tokyo

Shintaro Go

RIKEN Nishina Center

Chiara Mazzocchi

Faculty of Physics, University of Warsaw https://orcid.org/0000-0003-2503-5413

James Allmond

Oak Ridge National Laboratory https://orcid.org/0000-0001-6533-8721

Aleksander Augustyn

National Centre For Nuclear Research https://orcid.org/0009-0007-3055-1179

Nico Braukman

Universtity of Tennessee, Knoxville https://orcid.org/0009-0000-4666-0440

Pierre Brionnet

RIKEN Nishina Center

Arwin Esmaylzadeh

Universitat zu Köln https://orcid.org/0000-0003-0408-3774

Julia Fischer

Institut für Kernphysik, Universität zu Köln

Gabriel Garcia de Lorenzo
Universidad Complutense de Madrid

Shutaro Hanai
University of Tokyo, Center for Nuclear Study

Donnie Hoskins III
University of Tennessee, Knoxville

Nobuaki Imai
the University of Tokyo https://orcid.org/0000-0001-8864-369X

Kay Kolos
Lawrence Livermore National Laboratory

Agnieszka Korgul
Faculty of Physics, University of Warsaw https://orcid.org/0000-0003-0316-170X

Ben Kreider
University of Tennessee, Knoxville

Shin'ichiro Michimasa
RIKEN Nishina Center

Katsuhisa Nishio
Japan Atomic Energy Agency (JAEA)

Vi Phong
RIKEN Nishina Center

Thomas Ruland
Oak Ridge National Laboratory

Hiroyoshi Sakurai
RIKEN https://orcid.org/0000-0002-6215-4254

Yohei Shimizu
RIKEN Nishina Center

Aleksandra Skruch
University of Warsaw https://orcid.org/0009-0001-3638-1576

Hiroshi Suzuki
RIKEN

Hiroyuki Takeda
RIKEN

Y. Togano
RIKEN Nishina Center

Zhengyu Xu
University of Tennessee, Knoxville https://orcid.org/0000-0001-8626-1276

Masahiro Yoshimoto
RIKEN Nishina Center

Physical Sciences - Article

Keywords:

Posted Date: November 17th, 2025

DOI: https://doi.org/10.21203/rs.3.rs-7991707/v1

Additional Declarations: There is **NO** Competing Interest.

Direct observation of the superallowed α decay of ^{104}Te

Ian Cox[1*], Robert Grzywacz[1*], T. T. King[2], K. P. Rykaczewski[2], S. Nishimura[3], R. Yokoyama[4], N. Fukuda[3], N. Kitamura[4], S. Go[3], C. Mazzocchi[5], J. M. Allmond[2], A. Augustyn[6], N. Braukman[1], P. Brionnet[3], A. Esmaylzadeh[7], J. Fischer[7], G. Garcia de Lorenzo[8], S. Hanai[4], D. Hoskins[1], N. Imai[4], K. Kolos[9], A. Korgul[5], B. Kreider[1], S. Michimasa[3], K. Nishio[10], V. Phong[3], T. J. Ruland[2], H. Sakurai[3], Y. Shimizu[3], A. Skruch[5], H. Suzuki[3], H. Takeda[3], Y. Togano[3], Z. Y. Xu[1], M. Yoshimoto[3]

[1*]Department of Physics and Astronomy, University of Tennessee, Knoxville, TN, 37996, USA.
[2]Physics Division, Oak Ridge National Laboratory, Oak Ridge, TN, 37831, USA.
[3]RIKEN Nishina Center, 2-1 Hirosawa, Wako-shi, Saitama, 351-0198, Japan.
[4]Center for Nuclear Study (CNS), University of Tokyo, Wako-shi, Saitama, 351-0198, Japan.
[5]Faculty of Physics, University of Warsaw, PL 02-093, Warsaw, Poland.
[6]National Centre for Nuclear Research, Pasteura 7, 02-093, Warsaw, Poland.
[7]Institut für Kernphysik, Universität zu Köln, 50937, Köln, Germany.
[8]Grupo de Física Nuclear, Universidad Complutense de Madrid, E-28040, Madrid, Spain.
[9]Lawrence Livermore National Laboratory, Livermore, California, 94550, USA.
[10]Advanced Science Research Center, Japan Atomic Energy Agency (JAEA), 2-4 Shirakata, Tokai, Ibaraki, 319-1195, Japan.

*Corresponding author(s). E-mail(s): iancox02@gmail.com; rgrzywac@utk.edu;

Abstract

Alpha particle radioactivity is one of the most striking evidence for the existence of cluster structures in atomic nuclei. During the decay process, a preexisting $\boldsymbol{\alpha}$ particle tunnels through the potential barrier formed by the residual nucleus [1, 2]. The degree of preformation of the $\boldsymbol{\alpha}$ particle, a strongly bound system of two protons and two neutrons, is extracted from the data by dividing the $\boldsymbol{\alpha}$-decay probability by the barrier penetrability for a given particle energy. The preformation probability changes rapidly near nuclear shell closures, which is direct evidence that clustering is connected to nuclear structure [3]. Enhanced preformation was observed in the lightest $\boldsymbol{\alpha}$-particle emitters, spherical tellurium and xenon isotopes decaying to magic isotopes of tin. Here, we show the most extreme case of $\boldsymbol{\alpha}$-particle preformation from the measurement of the decay of tellurium-104. With a half-life of $\mathbf{7.2^{+2.3}_{-1.5}}$ nanoseconds, tellurium-104 is the fastest ground state $\boldsymbol{\alpha}$-emitting nucleus known to date. The deduced preformation demonstrates that the enhancement is greater for tellurium-104 than for any other nucleus. One nuclear model that can explain our observation postulates that the $\boldsymbol{\alpha}$ particle can exist only in the low nuclear matter density regions on the surface of the nucleus. The uniquely high preformation for tellurium-104 is attributed to its relation to doubly-magic tin-100, creating conditions conducive to form an $\boldsymbol{\alpha}$ particle.

1 Introduction

Alpha (α) particle emission is the oldest known type of radioactivity [4] and is the dominant decay mode for hundreds of nuclei including most known super-heavy elements. Consisting of two protons and two neutrons (^{4}He nucleus), the α particle has a binding energy of 7.074 MeV/nucleon and is the most bound system before ^{12}C [5]. Due to its strong binding, a ^{4}He nucleus exhibits the properties of an elementary charged particle. This allows for the formation of well-known α-cluster structures in excited states of light nuclei, such as the Hoyle state in ^{12}C which is crucial for the formation of elements beyond carbon [6]. The tightly bound nature of α particles leads to α radioactivity in heavier nuclei (mass $A > 100$), which are unbound against α-particle emission due to a positive decay energy ($Q_\alpha > 0$). The formation of the α particle prior to decay provides compelling evidence for cluster formation in heavy nuclei, but there is no consensus on the nature of this process. In fact, more than one and a quarter of a century after the discovery of α-radioactivity, the exact mechanism of α-particle appearance in the nucleus before emission remains unknown. Unlike light α-cluster systems, the α-decaying nuclei are known to have relatively uniform distribution of protons and neutrons inside the nucleus with a near constant nuclear density of 0.6 nucl/fm^3. Little is known about α clustering in heavier nuclei, with only a recent observation of α clustering using proton induced α-knockout reactions [7]. In addition, clustering has not been observed as a prevalent self-organization mode for known precursors. In the formative days of quantum mechanics, Gamow and, independently, Gurney and Condon explained the emission process as an example of the tunneling of a charged particle through a potential barrier [1, 2]. Charged particle emission from nuclei is well understood, and the tunneling model can successfully describe the 31 order-of-magnitude variations in the nuclear lifetimes observed for known α emitters. However, the validity of this model relies on the postulate of the α particle before it is emitted. Leaving the question, how is the α particle formed within the relatively homogeneous nucleus? In attempts to address this question, two emitters are of particular importance, because they can be pictured as elementary systems of a doubly-magic nucleus and an α particle; these are the classic case of ^{212}Po (^{208}Pb+α) and the almost unknown ^{104}Te (^{100}Sn+α). While a number of studies have centered on describing α clustering in ^{212}Po, there are strong indications in experimental data and theoretical predictions that α-particle preformation in ^{104}Te is the strongest among all nuclei, hence it is uniquely suited to understand the nature of α-particle emission.

Historically, the success of the Geiger-Nuttall law, which related the half-life to the α energy [8], is due to potential barrier tunneling acting as the dominant mechanism driving α radioactivity. Preformation effects are only quantified when the energy dependence for the potential barrier penetration is removed. Rasmussen introduced a method to measure the preformation of the α particle using the reduced width, $\delta^2 = h\lambda/P$, where h is Planck's constant, λ is the partial α-decay constant and P is the barrier penetrability [3]. Using the Gamow model, the barrier penetrability can be quantified for a given shape of the potential barrier and decay energy, Q_α. The resulting reduced widths revealed strong variations when plotted as a function of the neutron, N, and proton, Z, numbers. Curiously, nuclear shells proposed by Mayer [9] and independently by Haxel [10] were found to impact the reduced width. An increase in α preformation after the $N = 126$ shell closure was noted already by Rasmussen [3]. This provided clear evidence that the nuclear shell structure not only influences α decay by affecting Q_α but also by impacting the preformation. Shortly after, Mang made the first attempt to calculate the preformation using a newly developed shell-model for the series of even-even Po ($Z = 84$) nuclei ($A = 202-218$) in the vicinity of the doubly-magic ^{208}Pb. The calculations reproduced a variation in the reduced widths as a function of neutron number with a stronger preformation for $^{212-218}$Po [11]. While providing the first theoretical explanation for the variations of α preformation, Mang's values under-predicted the reduced widths.

Later, the island of lighter α-emitters was discovered in $N \approx Z$ isotopes of xenon ($Z = 54$) and tellurium ($Z = 52$), with much stronger preformation than in the ^{208}Pb region [12]. Macfarlane coined the term "superallowed α-decay," postulating the enhanced α-particle preformation for self-conjugate ($N = Z$) nuclei. This increase was attributed to the shell structure of these nuclei, where protons and neutrons occupy the same orbitals, allowing pairing forces to create α particles from overlapping proton and neutron wavefunctions. The same authors made a radical prediction that ^{104}Te will be a unique example of such superallowed decay, being a system that consists of an α particle and the doubly-magic ^{100}Sn [12]. Since then, a large body of experimental and theoretical work has been committed to study nuclei near ^{100}Sn [12–19]. Experiments found more cases with moderate increase of preformation, while theoretical models have evolved to a very high level of sophistication in an attempt to reproduce the experimental results [20–32]. ^{104}Te is considered to be unique and the most important system to investigate the nature of α cluster formation before it's emission. This manuscript presents a definite measurement of the lifetime of this nuclide and demonstrates that it is not only the shortest-lived α particle emitter, but also the nucleus with the highest probability of α-particle preformation. With a substantially enhanced reduced width, the "superallowed" nature of ^{104}Te α decay is verified.

2 Production and Identification of RI Beams

The synthesis of ^{104}Te in nuclear reactions is extremely challenging and became possible only recently using advanced technologies. Early systematic predictions of $\sim$50 ns for the ^{104}Te lifetime eliminated the option of direct observation of this isotope using electromagnetic separators because it is too short-lived. Therefore the

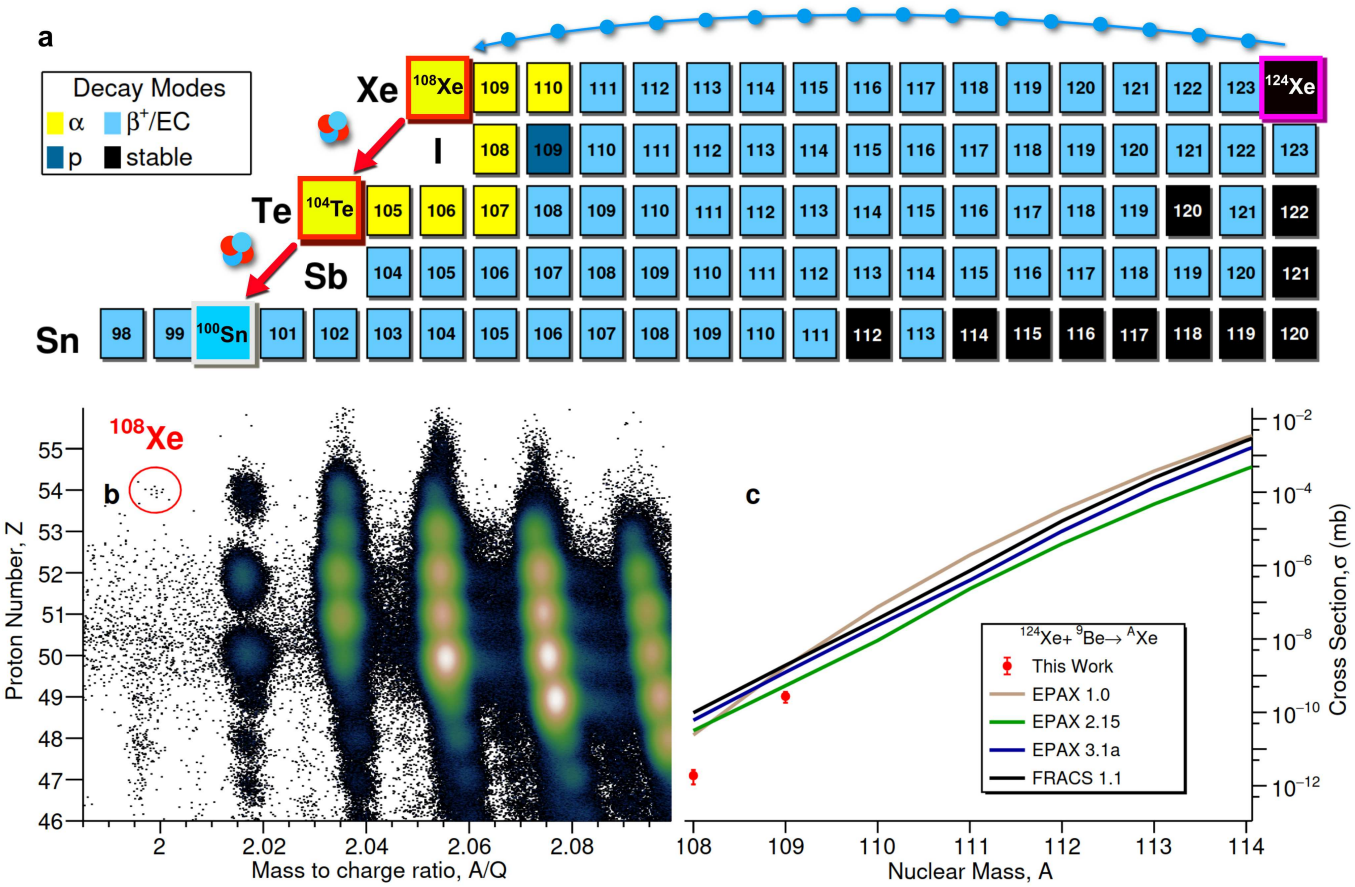

Fig. 1 (a) Primary decay modes for proton-rich nuclei with $50 \leq Z \leq 54$, produced via the fragmentation of ^{124}Xe (highlighted by the pink box). This work focuses on the production and implantation of ^{108}Xe (red box) to study the α decay chain through ^{104}Te to ^{100}Sn, shown by the red arrows. (b) Particle identification of fragments traveling through the BigRIPS separator, gated on implants in the LYSO detector. Events corresponding to the desired ^{108}Xe nucleus are within the red circle. (c) shows the cross-section predictions for the fragmentation of ^{124}Xe to produce isotopes of Xe. Highlighted in red are the results from this work for ^{108,109}Xe, which are significantly lower than predictions.

prior attempts focused on producing the longer lived ^{108}Xe, which is the α-decay precursor for ^{104}Te. As the heaviest known $N = Z$ nucleus, ^{108}Xe is also extremely difficult to create. Previous efforts to synthesize nuclei in the ^{100}Sn island of α radioactivity used fusion-evaporation reactions, such as ^{58}Ni+^{54}Fe, but reached the limit of the method's capabilities [18]. Instead, this work chose fragmentation of relativistic ^{124}Xe to produce ^{108}Xe. While the fragmentation reaction cross section is much lower than the ∼1 nb observed in the traditionally used fusion-evaporation reactions, fragmentation of ^{124}Xe enables the use of a thick target, providing an improvement of the total luminosity of the reaction. This experiment was performed at the Radioactive Ion Beam Factory (RIBF) at RIKEN. A primary beam of ^{124}Xe, highlighted by the pink box in Figure 1a, was accelerated by four coupled cyclotrons to a final beam energy of 345 MeV/nucleon and an average intensity of 120 particle nanoampere (pnA). Proton-rich fragments were created after the xenon beam impinged on a 6 mm thick ^{9}Be production target, before purification by the BigRIPS fragment separator [33]. Products were identified on an event-by-event basis using the $\Delta E - B\rho$−time of flight (ToF) method and transported to the implantation and spectroscopy station. The resulting particle identification plot is shown in Figure 1b. It shows a group of 12 counts unambiguously identified as ^{108}Xe fragments measured over the course of 124 hours. In this reaction, 16 neutrons were removed from ^{124}Xe. Using the estimated transmission of 39% from LISE++ [34], a production cross section of $1.89(0.5)_{\rm stat}(0.38)_{\rm sys}$ femtobarns (fb) was extracted for ^{108}Xe and $273(6)_{\rm stat}(55)_{\rm sys}$ fb for ^{109}Xe resulting from a transmission of 34%. These results are shown in Figure 1c and are consistently lower than model predictions from EPAX and FRACS [35–38]. The cross section of ^{108}Xe is one of the lowest production cross-sections since the identifications of ^{39}Na and ^{60}Ca at 0.5 and 0.21(0.15) fb, respectively [39, 40]. More details on the production can be found in the Methods.

3 Observation of the α-decay chain

Due to its short lifetime, the detection of ^{104}Te relies on the observation of the ^{108}Xe → ^{104}Te → ^{100}Sn decay chain, utilizing the pileup method demonstrated by the discovery of the ^{109}Xe → ^{105}Te → ^{101}Sn decay chain [17, 42]. Namely, the electronic signal induced by two consecutive interactions in the detector is captured using a digital data acquisition system. In this experiment, a detection system similar to that implemented by

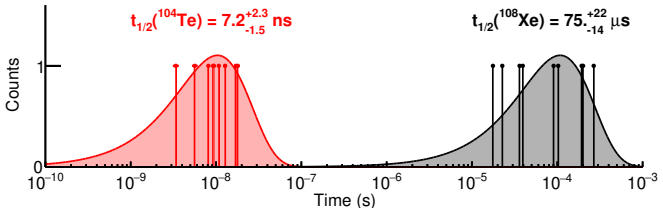

Fig. 2 Half-life measurements for ^{108}Xe (black) and ^{104}Te (red), extracted using the likelihood method described by Schmidt et al. [41]. The resulting half-life of ^{104}Te marks the fastest ground-state α emission.

Ref. [19] was used, employing fast-response scintillator detectors in anticipation of the short nanosecond scale half-life of ^{104}Te. Radioactive ions were implanted into a 0.6 mm thick LYSO ($Lu_{1.8}Y_{0.2}SiO_5$:Ce) inorganic scintillator coupled to a Hamamatsu H12700B-10 multi-anode photomultiplier tube (MAPMT) [19, 43, 44]. Surrounding the implant detector were sixteen 2-inch $LaBr_3$ based γ-ray detectors [45] arranged in a barrel configuration for isomer identification, $\alpha - \gamma$ coincidence measurements, and background rejection. Signals from the $LaBr_3$ and LYSO detectors were digitized using XIA Pixie-16 14-bit 500 MHz digitizers [46]. Digitized signals were stored and analyzed using C++ and the ROOT analysis framework [47]. See the Methods for more information on the implant and decay measurements.

Nine ^{108}Xe decays were correlated with the 12 ion implantations, leading to a correlation efficiency of 75%, consistent with other xenon and tellurium isotopes in the beam setting. See Table 2 in the Methods for more information. None of the ^{108}Xe events were measured in coincidence with a γ-ray in the surrounding $LaBr_3$ array, and their time distribution relative to the identified ion implantation is shown in Figure 2 by the black points. The half-life of ^{108}Xe was determined to be 75^{+22}_{-14} μs with a confidence of 68% using the likelihood method [41], which is in agreement with the previous measurement of 58^{+106}_{-23} μs from Auranen et al. [18]. In the same measurement, the ^{104}Te lifetime was estimated to be less than 18 ns [18]. ^{104}Te is populated in the decay of ^{108}Xe, where the first and second α's are measured in a short time window. With a fast lifetime, the signal from the second α is "piled-up" on the first α signal, creating a sum of the two decays. Details on the pileup deconvolution method are described in the Detector Response Methods section. From the ^{108}Xe events, the time difference between the two pileup decays shown by the red points in Figure 2. The half-life of ^{104}Te was determined to be $7.2^{+2.3}_{-1.5}$ ns using the same likelihood method as for ^{108}Xe [41]. This value is nearly a factor of 8 faster than ^{219}Pa [48], making ^{104}Te the fastest ground state α-decaying nucleus known.

The amount of light produced for each decay was obtained from the signal amplitude. Calibrations were performed internally using known α-emitters $^{105-107}$Te, ^{109,110}Xe, and a standard ^{210}Po source. More details on the detector calibration can be found in the Methods. The α energies were measured to be 4.64(9) MeV for ^{108}Xe and 5.03(9) MeV for ^{104}Te. These values are in agreement with the previously reported 4.4(2) MeV and 4.9(2) MeV for ^{108}Xe and ^{104}Te, respectively [18]. Correspondingly, the Q_α values are determined to be 4.82(9) MeV for ^{108}Xe and 5.23(9) MeV for ^{104}Te.

4 Experimental evidence for super-allowed α decay

With the measured half-life and α-decay energy, the reduced widths were extracted for each decay using the WKB approach. For ^{104}Te, the reduced width is $0.82^{+1.07}_{-0.46}$ MeV. The uncertainty of this value is dominated by the energy uncertainty resulting from the choice of experimental method, which was optimized for half-life measurement. Figure 3a shows this value compared to all other known even-even ground-state α-emitters. A large amount of the nuclei decay with a reduced width between 0.1 and 0.3 MeV, with ^{104}Te towering above the rest. This serves as the first indication of the unique nature of the ^{104}Te decay. Also in the $N \approx Z$ region, the decay of ^{114}Ba produces a large reduced width, yet with conflicting decay energies between two measurements [49, 50] and large uncertainly on the α branching ratio, the reduced width may be inflated. The reduced width of ^{108}Xe was found to be $0.02^{+0.05}_{-0.01}$, which is in agreement with the previous value of $0.27^{+2.0}_{-0.24}$ [18]. The enhancement of ^{104}Te relative to its $N = Z$ counterpart illuminates that the superallowed nature of ^{104}Te is not solely due to self-conjugate nature of the nucleus.

The difference in α-particle preformation in the ^{100}Sn and ^{208}Pb regions can be observed by investigating the reduced width when approaching the neutron shell closure, as shown in Figure 3b with $N_{\text{magic}} = 50, 126$ for the tin and lead regions, respectively. Approaching the $N - N_{\text{magic}} = 0$ line, the reduced widths of tellurium isotopes steadily increase. This behavior differs from the polonium decays, which have a relatively constant reduced width when decreasing in neutron number to ^{212}Po. The change in systematics indicates that, while the two systems are qualitatively similar, the α formation mechanism differs significantly between the two regions.

Historically, reduced widths are compared to ^{212}Po due to its simplicity, yielding the preformation factor, $W_\alpha = \frac{\delta^2}{\delta^2(^{212}\text{Po})}$. This provides direct comparison to the only other α-emitter decaying to a doubly-magic nucleus. Auranen et al. claimed a lower limit of 13.1 on the preformation factor of ^{104}Te due to the relatively small Q_α = 4.9(2) MeV and $t_{1/2} < 18$ ns [18]. The present result of $W_\alpha = 11.7^{+15.5}_{-6.5}$ is smaller than previously reported lower limit due to a higher central value for the decay energy. However, because the decays of ^{108}Xe and ^{104}Te could not be disentangled in the previous measurement, a broad range of solutions were possible for $W_\alpha(^{108}\text{Xe})$ and $W_\alpha(^{104}\text{Te})$, see Fig. 5 in [18]. The only definitive claim is that one of the nuclei in the decay chain is more than 5 times enhanced relative to ^{212}Po [18]. Thus, this work provides the first proof of the "superallowed" nature of the ^{104}Te decay, with a reduced width which is at least one order of magnitude larger than ^{212}Po.

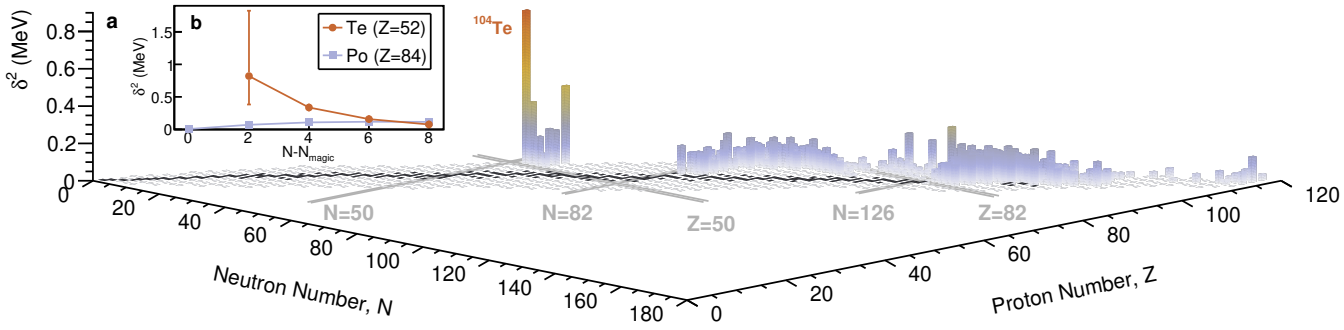

Fig. 3 (a) The reduced width centroid values, δ^2, for known even-even α-emitters [5] calculated using the WKB formalism described in [3]. ^{104}Te is seen as the most preformed α decay with the largest reduced width across the chart of nuclei. (b) Decays from tellurium (orange) to tin isotopes and polonium (light blue) to lead isotopes approaching neutron shell closures at $N_{\rm magic} = 50,\ 126$, respectively. The unique nature of tellurium isotopes is seen as the reduced width increases up to the decay into the doubly-magic ^{100}Sn. Alternatively, the polonium isotopes have a relatively flat reduced width above the shell closure.

5 Discussion

The measurement of the ^{108}Xe $\rightarrow$ ^{104}Te $\rightarrow$ ^{100}Sn decay chain provides evidence not only for the shortest ever measured α-decay lifetime, but also for the strongest α preformation. This confirms the singular nature of its decay, which in that sense is indeed "superallowed" as postulated by MacFarlane and Siivola. In order to fully understand the depth of this discovery, we must consult theoretical models, which for several decades have tried to predict the properties of this particular nucleus and explain the origin of the expected enhancement of the decay using state-of-the-art nuclear models. The location of ^{104}Te close to ^{100}Sn, which is a confirmed doubly-magic nucleus [51–53], eliminates the enhancement scenario of this decay due to changes in the nuclear potential caused by deformation and allows for the simple picture of ^{104}Te as a ^{100}Sn core with an α particle. Figure 4 shows the experimental comparison to several theoretical models, shown as a blue histogram [20–24, 26–28, 30–32, 54] compared to the result of this work in orange. Many models report calculated preformation factors relative to ^{212}Po, in this case the value from the reference was used [22, 24, 26, 30]. Otherwise, the preformation factor was calculated using the WKB formalism from the reported half-life and decay energy in each respective published research [20, 21, 23, 27, 28, 31, 32, 54].

It is clear that nearly all models underpredict the preformation. The large body of models using implicit clusters require such empirical parameterizations of existing experimental data and thus do not include more fundamental physics considerations. But even fully microscopic models, which generally emerge the α-particle from the parent nucleus configuration, are too conservative, perhaps for similar reasons.

Microscopic models aim to describe the α-particle preformation as an emergence from nuclear configurations. In the pioneering calculations performed for polonium nuclei by Mang [11], the preformation was generated from the α cluster overlap with shell-model configurations of valence protons and neutrons. While the calculations were able to reproduce trends across shell closures and showed a direct link between nuclear structure and α particle formation, the absolute α-decay widths were under predicted. Similar calculations were later utilized for ^{104}Te, employing the complex-energy shell model (CESM) [23] and the multistep shell model (MSM) [24]. Both CESM and MSM produced lifetimes which are more than 100$\times$ larger than the value determined by this work, with the CESM discrepancy expected due to proton continuum effects and the lack of proton-neutron (pn) correlations [23]. The MSM produced a relative α preformation of ^{104}Te 4.85$\times$ larger than that of ^{212}Po attributed to pn correlations, but the model is incomplete with an insufficiency in cluster components yielding an absolute formation amplitudes at least two orders of magnitude too small [24]. Baran and Delion reached the conclusion that pn correlations are not sufficient to explain the large under prediction of the reduced width for $N \approx Z$ nuclei [25]. While the effect of pn correlations remains unsolved, several authors concluded that the α particle must form on the edge of the nucleus. The key insight of the quartetting wave function approach (QWFA) was the introduction of four-body correlations, called quartetting [55, 56]. In the approach, α-particles can only form on the surface of the nucleus where the nuclear density was less than the saturation density and the cluster correlation does not survive in the interior of the nucleus [57]. The QWFA was implemented to describe clusterization in the classic low-mass cases [58, 59] and was later employed to describe α-radioactivity in the ^{208}Pb region [57, 60]. The effects of cluster formation on the nuclear equation of state were studied by Typel [61], and more recently were used to interpret experimental results using proton induced α-knockout reactions on stable tin isotopes, which inferred α-clustering in heavy nuclei [7]. The QWFA was improved with the addition of structure information for the core nucleus from nucleon-nucleon interactions and calculations extended to ^{104}Te [26]. These changes naturally incorporated the shell structure and predicted a roughly 6 times increase in the preformation in ^{104}Te compared with ^{212}Po, as well as predicted a short half-life of 14.8 ns [26]. As the only theoretical prediction with a preformation greater than 5, as seen in Figure 4, the QWFA model is the only model in agreement with the experimental results of this work. The

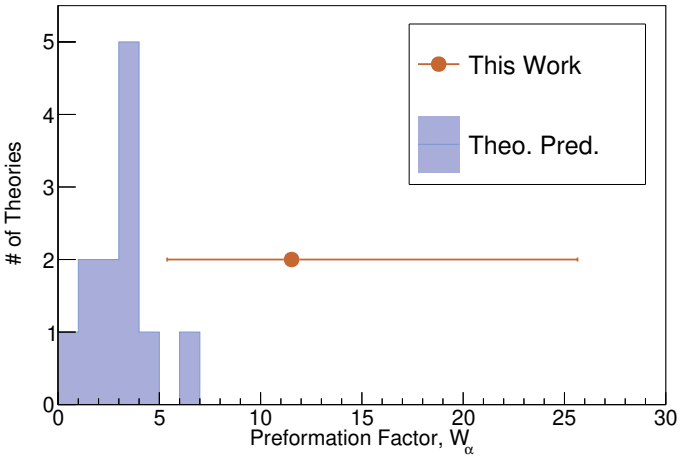

Fig. 4 Comparison of theoretical predictions (blue) [20–24, 26–28, 30–32, 54] for the preformation factor, W_α, of ^{104}Te with experimental results from this work (orange). Nearly all models underpredict the preformation factor of ^{104}Te, with the exception being the Quartetting Wave Function Approach [26].

QWFA is the most successful in predicting the large preformation, but also in providing a direct connection to nuclear structure. The same authors have shown how the difference between valence proton and neutron configurations generates differences between predictions for the α preformations and decays ^{212}Po and ^{104}Te [29]. In this model, the contribution of the nuclear wavefunctions on the surface of the nucleus is critical to the formation of the alpha particle. With the inclusion of nuclear wavefunctions, sensitivity to the density of nuclear matter, and availability of protons and neutrons, the QWFA model can reproduce ^{212}Po properties using the same set of parameters as for ^{104}Te. This further indicates that the QWFA captures correctly the sensitivity of the α-particle preformation to the shell-model prediction of the density of the nuclear matter on the surface of the nucleus.

6 Conclusion

This work presents the first measurement of the half-life and an increase in precision for the decay energy of ^{104}Te, produced via the decay of the heaviest known $N = Z$ nucleus, ^{108}Xe. ^{104}Te was found to be the fastest ground-state α-emitting nucleus, and its "super-allowed" nature has been confirmed with the largest reduced width for any known α decay. The preformation factor was found to be 11.7 times stronger than that of ^{212}Po and comparisons with its $N = Z$ counterpart, ^{108}Xe, indicate that the observed effect is linked to its proximity to ^{100}Sn and not solely its self-conjugate nature. Among many model predictions, the closest to the experiment is from the QWFA model, which postulates that the α particle forms on the surface of the nucleus in the region of low-matter density. The sensitivity of the α-particle formation to the proton/neutron ratio and the relation to ^{100}Sn explains the exceptional character of ^{104}Te and the agreement with theory is compelling. The improvement of radioactive ion beam facilities may allow further studies using the $(p, p'\alpha)$ reaction in inverse kinematics to investigate the properties of α-radioactive nuclei. The small production cross-section of ^{108}Xe and short-half life of ^{104}Te made this measurement exceptionally challenging. The experiment focused on lifetime-measurement, sacrificing the energy resolution and introducing a large uncertainty in extracting of the preformation factor. Future measurements will have to address these challenges to provide more accurate experimental value of the preformation factor, which will be needed to better constrain and guide nuclear models.

7 Methods

7.1 Production of ^{108}Xe

^{108}Xe was produced via the fragmentation of ^{124}Xe on a ^{9}Be target. Products were identified on an event-by-event basis between the F3 and F7 focal planes of BigRIPS using the $\Delta E - B\rho$−time of flight (ToF) method and transported to the F11 focal plane for implantation into a spectroscopy station [33]. Generally, this type of reaction is used to produce $Z \lesssim 50$ nuclei, such as ^{100}Sn, and consequently the experimental data for the production of xenon ($Z = 54$) nuclei is sparse. Up to this point, the cross section was only measured out to ^{115}Xe at GSI [62], using a higher beam energy of 1 GeV/u. Accordingly, estimations for the production of ^{108}Xe from ^{124}Xe relied on fragmentation models. Predictions from EPAX [35–37] and FRACS [38] placed the expected cross section between 20 and 100 fb. However, the uncertainty of the reaction cross-section predictions prior to this experiment was considerable and reached a factor of 100 based on a study of $50 < Z < 52$ nuclei at RIBF [63].

The experimental cross section was extracted using a comparison to LISE++ predictions for the transmission of nuclei after fragmentation. To accurately estimate the transmission through the BigRIPS separator, the D1 dipole magnet was adjusted in LISE++ such that the calculated momentum distribution for ^{109}Xe matched the experimental distribution at the F5, momentum-dispersive, focal plane. The resulting predicted transmission through the BigRIPS separator was 39% for ^{108}Xe and 34% for ^{109}Xe. A standard 20% uncertainty was applied to account for the error in transmission from LISE++. Subsequently, the ^{108}Xe cross-section up to the F7 focal plane was found to be $1.89(0.5)_{\text{stat}}(0.6)_{\text{sys}}$ fb, and is significantly lower than the model predictions, as shown by Figure 1c. Additionally, for ^{109}Xe, the cross section was measured to be $273(6)_{\text{stat}}(90)_{\text{sys}}$ fb. This was also lower than the predictions by EPAX.

7.2 Detector Setup

The decay system hinged on the LYSO scintillator-based implantation detector. Figure 5 shows the experimental setup, with the LYSO shown in orange coupled to a segmented light guide and the MAPMT. Directly in front of the LYSO is a plastic detector used to track incoming ions and reject decay particles which leave the LYSO. Additionally, behind the MAPMT is a second plastic veto detector which rejects light ions that do not implant into the LYSO. Surrounding the central detectors are 16 $LaBr_3$ detectors, where the 2" cylindrical scintillators are shown as gray in Figure 5. These detectors were packed as close to the LYSO as possible to maximize the geometrical efficiency.

The MAPMT consisted of an 8×8 array of anodes, resulting in 64 anode signals and 1 additional dynode signal. Using the Vertilon SIB064B-1902 [64], a resistive readout array, these 64 anodes were reduced to 4 corner signals [43]. From these 4 signals, the position of an event can be reconstructed using Equation 1 with millimeter precision.

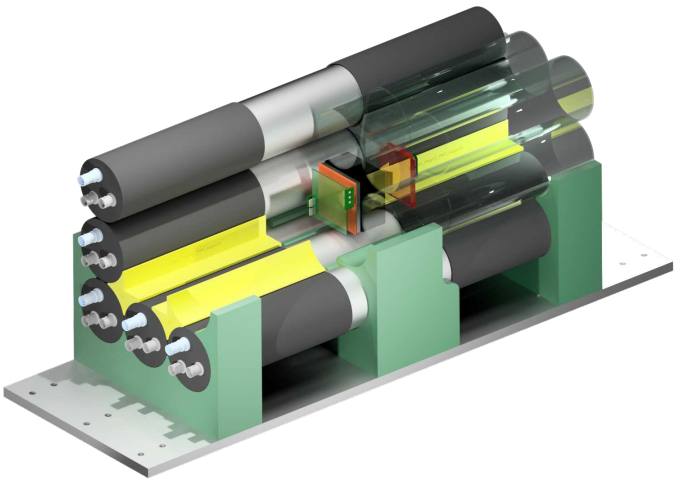

Fig. 5 The implantation setup used to stop the energetic ion beam and measure the subsequent decays. For illustrative purposes, some of the outside $LaBr_3$ detectors are transparent glass in order to view the implantation configuration. In the figure, the radioactive ion beam comes from the bottom left to implant into the LYSO, depicted as the orange square.

$$x_{\text{pos}} = \frac{(v_1 + v_2) - (v_3 + v_4)}{v_1 + v_2 + v_3 + v_4}$$
$$y_{\text{pos}} = \frac{(v_1 + v_4) - (v_3 + v_2)}{v_1 + v_2 + v_3 + v_4} \quad (1)$$

In this setup, the LYSO detector measures a large ion implantation signal with a total kinetic energy exceeding 1 GeV and a small signal induced by an α particle in quick succession. The was accomplished by operating two electronic gains, with the dynode (anode) decay signal(s) amplified by 20× (10×) before entering the digital data acquisition. Furthermore, within the data acquisition the implant signals were attenuated by an additional factor of 4. This 80× difference between implants and decays allows for the data acquisition to not be saturated during implant events, while also being able to measure the decays.

Large signals were deduced to be ion implantations when in coincidence with incoming particle identification from BigRIPS and no signal in a rear plastic detector. Subsequent α decays were measured by the same LYSO detector and correlated with ions of interest in space and time. Decay events are characteristically lower in energy, ≤ 10 MeV, and not in coincidence with any other beam-line detector from BigRIPS or the front and rear plastic detectors. This strict selection was used to isolate α decays that do not exit the LYSO.

7.3 Detector Response

The MAPMT dynode output is known to have an undershoot and ring for a short time after an implant or decay. Therefore to extract the energy from the pulse, a function, $F(t)$, determined by the convolution of a normal scintillator pulse, P, and a ring-like term, H, is used to fit

each individual trace. The result is defined in Equation 2.

$$
\begin{aligned}
F(t) &= (P * H)(t) \\
P(x) &= A(x > \phi)e^{-(x-\phi)/p_2}(1 - e^{-(x-\phi)/p_3}) \\
H(x) &= (x > p_4)\cos(p_6 x + p_7)e^{(-x-p_4)/p_5}
\end{aligned}
\tag{2}
$$

A wide range of decay signals were fit with all parameters free, with the resulting average values for parameters are shown in Table 1. These values were kept constant for the analysis, while only amplitude, A, and the phase, ϕ, remained free parameters. A sample fit result is shown in Figure 6(a). In the case of two decays occurring close in time, the sum of the two signals is produced in the dynode signal, leading to a "pileup" event. Two examples are shown from the decay chain of ^{108}Xe in Figure 6(b,c), where the blue curve is the fit for the first decay in the chain, corresponding to ^{108}Xe, the green curve corresponds to ^{104}Te, and the sum of the fit is shown as the pink curve. The 18 ns pileup, Figure 6(c), is clear with the decay time from the initial pulse being seen, but for faster pileup events, such as the 8 ns case shown in Figure 6(b), the indications of pileup are less clear. Visually, the risetime between the single event and the fast pileup can be compared, where there are nearly twice as many points on the risetime for the 8 ns pileup compared to the single event. This allows for a confident assignment of the event to a pileup signal.

After the individual trace is fit, its amplitude is used to determine the amount of light produced by the interaction. This light yield is calibrated to the 662 keV γ transition in ^{137}Cs standard source, with a resolution of $\sigma = 23$ keV electron equivalent (keVee) at 314 keVee for α decays. For the decay chain of ^{108}Xe, the resulting light yield measurements are shown in Figure 7 and fit using a binned likelihood method. Points greater than 5σ from the mean were excluded from the fits. The light yields for ^{108}Xe and ^{104}Te were found to be 366 ± 11 and 452 ± 20 keVee, respectively. Due to the error in amplitude resulting from the deconvolution, additional systematic errors were incorporated at 8.08 and 8.57 keVee for ^{108}Xe and ^{104}Te, respectively.

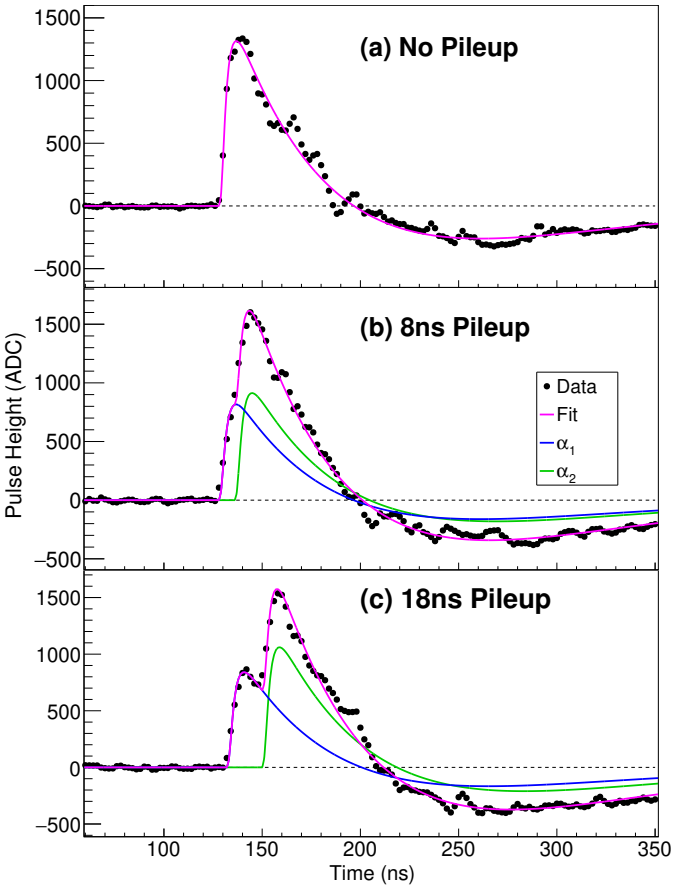

Fig. 6 Fits of a single peak (a), a pileup event with 8 ns time difference (b), and a pileup event with a 18 ns time difference (c). The pink curve is the total fit of the black experimental points, while the blue and green lines represent the decomposition in terms of the first and second decays, respectively.

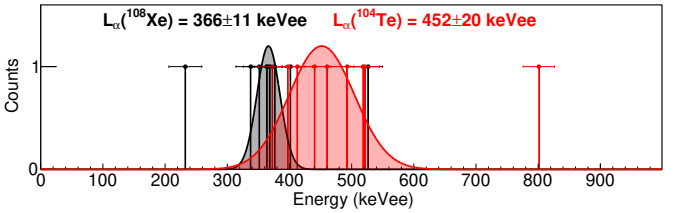

Fig. 7 Light yield measurements for the decay chain of ^{108}Xe (black) through ^{104}Te (red). Each point is marked with error from the resolution of the detector plus the error resulting from the trace deconvolution. Variations according to these errors are incorporated as the systematic errors.

7.4 Energy Calibration

Due to the fragmentation of ^{124}Xe, multiple less proton-rich α-emitting nuclei above ^{100}Sn were produced in high quantities, shown in Table 2. The number of implants and subsequent decays yields a correlation efficiency consistently above 70%, except in the case of ^{109}Xe, where correlations were restricted to events which could identify both the ^{109}Xe and ^{105}Te decays in the same trace. Due to a limited trace length of 1.8 μs after the initial signal, only 3 half-lives of ^{105}Te are able to be correlated to the initial ^{109}Xe decay, corresponding to 88% of the potential events. From this, a correlation efficiency of 68% was found for measuring both events, or 83% for a single correlation. Isotopes marked with a * represent decays to the first excited state in the respective daughter nucleus and are measured in coincidence with the corresponding γ ray.

In columns 5 and 6, the half-lives measured from this work are compared to literature values, where there is excellent agreement overall. In many cases, this work yields more precise measurements. The half-life of ^{105}Te is shorter in this work due to the event window length allowing for a maximum pileup time difference of 1.8μs. After this, some data is lost before the next event can occur. Additionally, the previous measurement was limited in its ability to measure fast pileups, $<$ 300 ns, leading to a bias towards a longer lifetime. A weighted average of the two measurements yields $t_{1/2}(^{105}\text{Te}) = 516 \pm 77$ ns. Additionally, this measurement of the half-life of ^{107}Te is higher than the literature, but earlier results

Table 1 Parameters used with the template function, Equation 2, to fit individual pulses.

A	ϕ	p_2	p_3	p_4	p_5	p_6	p_7
Free	Free	2.65856	4	-54.65	70.1454	-0.00747514	-1.49996

Table 2 List of implanted α-decaying nuclei, with their measured halflives. More details are in the text.

Isotope	# Imp.	# Decay	Corr. (%)	Half-life (sec)	Ref. Half-life (sec)	L_α (keVee)	$E_{\alpha,\mathrm{Lit}}$ (MeV)
^{108}Xe	12	9	75	$75^{+22}_{-14} \times 10^{-6}$	$58^{+106}_{-23} \times 10^{-6}$		
^{109}Xe	1659	996	83	$16.0(6) \times 10^{-3}$	$13(2) \times 10^{-3}$	297(2)	4.063(4)
^{110}Xe	29095	20757	71	$94(1) \times 10^{-3}$	$93(3) \times 10^{-3}$	274(1)	3.717(19)
^{104}Te		9		$7.2^{+2.3}_{-1.5} \times 10^{-9}$	$< 18 \times 10^{-9}$		
^{105}Te		996	83	$493(33) \times 10^{-9}$	$620(70) \times 10^{-9}$	421(4)	4.880(20)
^{105}Te*		X			$620(70) \times 10^{-9}$	362(2)	4.711(3)
^{106}Te	766308	602650	79	$67.9(1) \times 10^{-6}$	$70^{+20}_{-10} \times 10^{-6}$	314(1)	4.128(9)
^{107}Te	5024458	4185966	83	$3.532(3) \times 10^{-3}$	$3.1(1) \times 10^{-3}$	282(1)	3.853(13)
^{107}Te*		5144		$3.5(2) \times 10^{-3}$	$3.1(1) \times 10^{-3}$	265(2)	3.691(5)

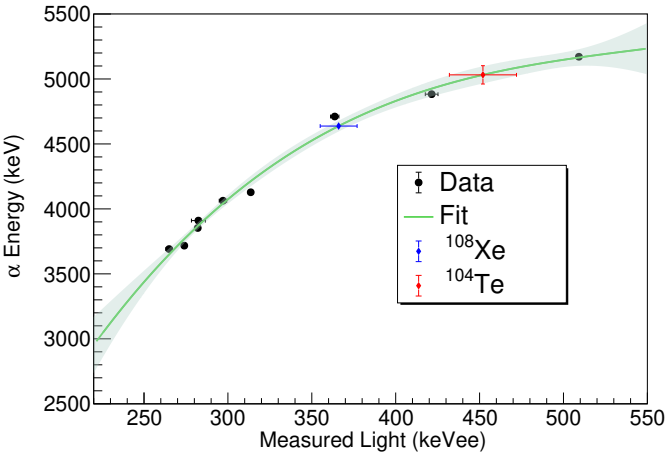

Fig. 8 Calibration from light yield to α decay energy using neighboring α emitters near ^{100}Sn and a ^{212}Po check source. The measured light yields for ^{108}Xe and ^{104}Te are shown by the blue and red points, respectively. The green band represents the error in the fit, which is propagated into the error in the α energy.

from Schardt [13] place the centroid of the half-life higher at $3.6^{+0.6}_{-0.4}$ ms

Lastly, columns 7 and 8 report the measured light yield of the α particles, L_α, in keVee and the literature value for the emitted α energy. Using the light output and known α energies, the detector is able to be calibrated to report α energies. Utilizing these points, along with data from a ^{210}Po check source, the LYSO detector is calibrated from light yield, L_α, to α-energy, E_α, using a third order polynomial, shown in Figure 8. The nonlinearity in the light produced by the LYSO is especially apparent for higher α energies, above 4.5 MeV. The α energy values for ^{104}Te (^{108}Xe) is show by the red (blue) point in Figure 8. The error in the α energy was calculated as a quadrature sum of the error in the fit, ε_f, and the propagation from the light yield, $\varepsilon_l = \left|\frac{\partial E_\alpha}{\partial L_\alpha}\right| \varepsilon_{L\alpha}$.

7.5 Extraction of Reduced Width

The formalism for the reduced width, δ^2, was introduced by Rasmussen in 1959 [3]. Using the WKB approximation, the penetrability, P, can be calculated for a given potential and energy using the equations from Ref. [3]. This formalism provides a consistent method to benchmark the reduced widths across the chart of nuclei, and also provides comparison against theories which use different Q_α values to predict α decay half-lives. Figure 9 shows the comparison of the reduced widths of Po isotopes calculated in this work (black circles) compared to the values originally reported by Rasmussen (red diamonds). The agreement is clear, indicating that these calculations are valid for reporting preformation factors.

To model the error for the reduced width, distributions for the half-life and Q_α were randomly probed as an input to calculate the reduced width. Figure 10 demonstrates this, where the Q_α distribution is shown in (a), the half-life distribution is shown in (d), and the combined input distribution for the reduced width is shown in (c). Lastly, (b) shows the resulting values for the reduced width. The $\pm 1\sigma$ errors were found using the 16$^{\mathrm{th}}$ and 84$^{\mathrm{th}}$ percentiles in the calculated distribution.

7.6 Theoretical Predictions

Multiple predictions of ^{104}Te properties originate from the Geiger-Nuttall law [8] and use the preformation of an

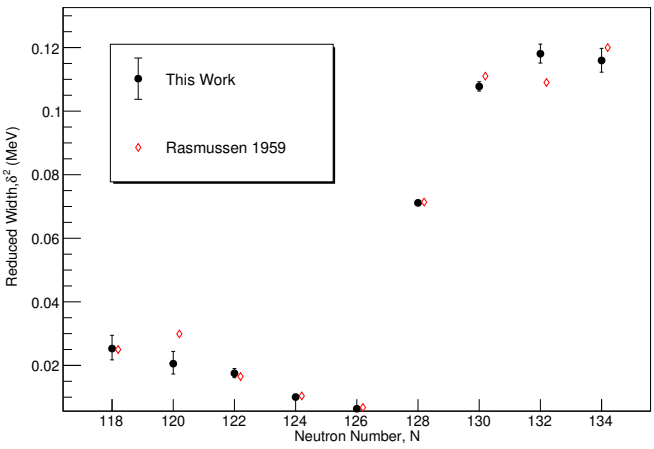

Fig. 9 Comparison of reported reduced widths from Rasmussen(red diamonds) [3] with those calculated for this work (black circles).

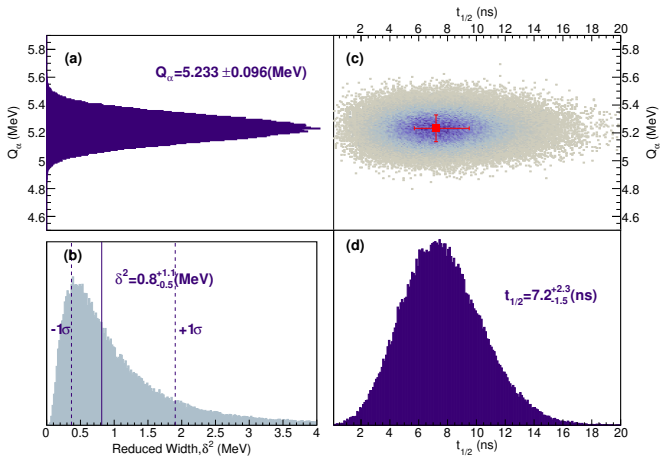

Fig. 10 Utilizing the decay energy (a) and half-life (d) distributions, an input distribution (c) is propagated into the reduced width calculations. The resulting error distribution for the reduced width is shown in (b).

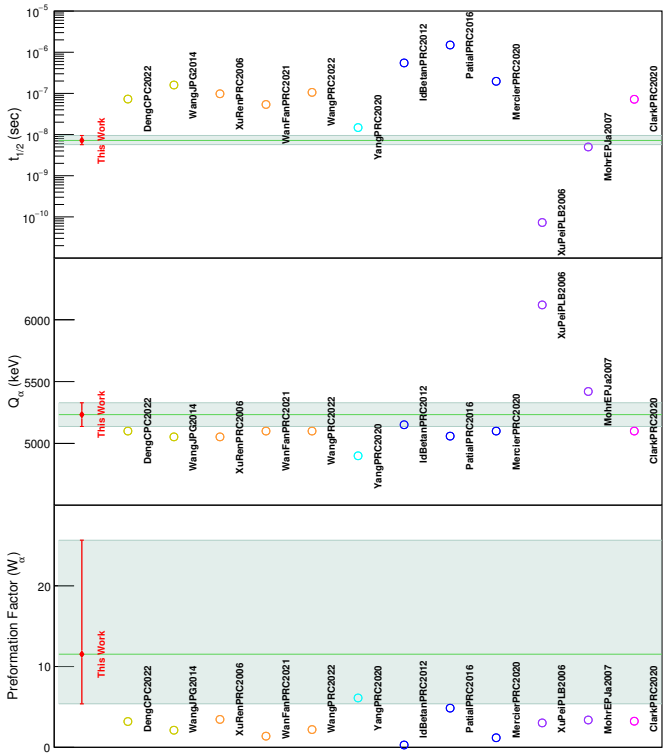

Fig. 11 Comparison of experimental (red) half-life, $t_{1/2}$, (top), Q_α (middle), and preformation factor, W_α (bottom), with theoretical predictions for the decay of ^{104}Te. Using theories [20–24, 26–28, 30–32, 54]. Most models underpredict the preformation factor, with the exception of Ref. [26]. The previous work by Auranen [18] is shown by the black points using the reported lower limit of 13.1, without error analysis.

α cluster as an empirically adjusted parameter to predict its decay probability. A few of these predictions are shown as the yellow circles [32, 54] in Figure 11. The predicted half-lives are significantly longer than the experimental result, leading to small preformations that contribute to the low-preformation bump in Figure 4.

The Density Dependent Cluster Model (DDCM), shown in orange in Figure 11, was developed assuming a symmetric α-core system with the preformation factor tuned as a free parameter [21]. More modern DDCM calculations have increased the complexity for preformation [30] or added a deformation dependence in the model [31], but neither of these progressions have been able to reproduce the decay of ^{104}Te, with the original model performing best. Other models have predicted the lifetime using a mean field analysis [20] or a double folding potential [22] and are shown in purple. Both predictions use large Q_α values, but still do not reproduce the α preformation. Clark et al., devised a model with a parametrized pairing gap, dependent on the proton to neutron asymmetry, which yields increased preformation factors for $N \approx Z$ nuclei compared to decays near ^{208}Pb [27]. Even with the increased preformation, the model underpredicts the preformation factor, as shown by the pink circle in Figure 11. A recent attempt to describe the decay of ^{104}Te using an energy density functional method also over-predicted the lifetime [28], resulting in a lower preformation, shown in blue in Figure 11. As mentioned in the text, microscopic models from Id Betan and Patial, shown in blue, over-predict the half-life of ^{104}Te [23, 24].

The QWFA, represented by the light blue circle [26] in Figure 11, begins by introducing the center-of-mass motion of the quartet and the relative motion of the quartet with respect to the core of the nucleus. This led to the introduction of an effective local pocket potential, which enabled preformation calculations for an a-priori nonlocal interaction between the quartet and the core. This pocket potential occurs at the edge of the nucleus, in the region where the nucleon density drops below the Mott-density [57]. Using this formalism, the clustering for ^{104}Te was found to be $\sim 6\times$ larger than that for ^{212}Po, calculated using the same framework. As a result, QWFA is the only theoretical model within 1σ of the experimental results presented in this work.

Data Availability

The data used in this work originates from experiment 168 at RIKEN RIBF. The raw data are available upon reasonable request.

Code Availability

The code used to analyze the data is available upon reasonable request.

Acknowledgements

We would like to thank the entire RIBF operations team. The material is based upon work supported in part by the U.S. Department of Energy, Office of Science, Office of Nuclear Physics under Contracts No. DE-FG02-96ER40983 (UTK) and DE-AC05-00OR22725 (ORNL), the auspices of the U.S. Department of Energy by Lawrence Livermore National Laboratory under Contract DE-AC52-07NA27344, and the Polish National Science Center under Grant No. 2020/39/B/ST2/02346 and contract No. UMO-2019/33/B/ST2/02908. This work was also sponsored by JSPS KAKENHI Grant No.

25H01273 and RIKEN program RiNA-Net, the Stewardship Science Academic Alliances program through DOE Awards No. DE-NA0003899 (UTK), and the National Science Foundation NSF-MRI- 1919735 (UTK). We would like to thank T. Papenbrock and K. L. Jones for helpful discussions.

Author contribution

R. G. and K. P. R. were the lead and co-spokesperson for the experiment, respectively. The design and installation was led by R. G., T. T. K., and I. C., with additional contributions from R. Y. and D. H. Supplemental equipment was provided by J. M. A., R. Y., and S. N. The data acquisition system and software was maintained by T. T. K., I. C., R. Y., Z. Y. X., T. J. R. and R. G. Online data monitoring and operation of the experiment was performed by I. C., R. G., T. T. K., K. P. R., S. N., R. Y., N. F., N. K., S. G., C. M., N. B., P. B., A. E., J. F., G. GdL, S. H., D. H., N. I., K. K., A. K., K. N., V. P., T. J. R., A. S., and Z. Y. X. The beam transportation was led by N. F., S. M., Y. S., H. S., H. T., Y. T., and M. Y. The offline analysis was led by I. C. with contributions from R. Y., Z. Y. X., A. A., and B. K. The manuscript was written by I. C. and R. G. All authors have read and commented on the manuscript.

Competing interests

The authors declare no competing interests.

References

[1] Gamow, G.: Quantum theory of the atomic nucleus. Zeitschrift für Physik **51**(2), 204–212 (1928)

[2] Gurney, R.W., Condon, E.U.: Quantum mechanics and radioactive disintegration. The Physical Review **33**(2), 127–140 (1929)

[3] Rasmussen, J.O.: Alpha-decay barrier penetrabilities with an exponential nuclear potential: even-even nuclei. The Physical Review **113**(6), 1593–1598 (1959)

[4] Rutherford, E.: Uranium radiation and the electrical conduction produced by it. The London, Edinburgh and Dublin Philosophical Magazine and Journal of Science **47**(284), 109–163

[5] Kondev, F.G., Wang, M., Huang, W.J., Naimi, S., Audi, G.: The nubase2020 evaluation of nuclear physics properties. Chinese Physics C **45**(3), 030001 (2021) https://doi.org/10.1088/1674-1137/abddae

[6] Hoyle, F.: On Nuclear Reactions Occuring in Very Hot STARS.I. the Synthesis of Elements from Carbon to Nickel. Astrophysical Journal Supplement **1**, 121 (1954) https://doi.org/10.1086/190005

[7] Tanaka, J., Yang, Z., Typel, S., Adachi, S., Bai, S., Beek, P., Beaumel, D., Fujikawa, Y., Han, J., Heil, S., Huang, S., Inoue, A., Jiang, Y., Knösel, M., Kobayashi, N., Kubota, Y., Liu, W., Lou, J., Maeda, Y., Matsuda, Y., Miki, K., Nakamura, S., Ogata, K., Panin, V., Scheit, H., Schindler, F., Schrock, P., Symochko, D., Tamii, A., Uesaka, T., Wagner, V., Yoshida, K., Zenihiro, J., Aumann, T.: Formation of α clusters in dilute neutron-rich matter. Science **371**(6526), 260–264 (2021) https://doi.org/10.1126/science.abe4688 https://www.science.org/doi/pdf/10.1126/science.abe4688

[8] Geiger, H., Nuttall, J.M.: Lvii. the ranges of the α particles from various radioactive substances and a relation between range and period of transformation. The London, Edinburgh, and Dublin Philosophical Magazine and Journal of Science **22**(130), 613–621 (1911) https://doi.org/10.1080/14786441008637156 https://doi.org/10.1080/14786441008637156

[9] Mayer, M.G.: On Closed Shells in Nuclei. II. Phys. Rev. **75**, 1969–1970 (1949) https://doi.org/10.1103/PhysRev.75.1969

[10] Haxel, O., Jensen, J.H.D., Suess, H.E.: On the "Magic Numbers" in Nuclear Structure. Phys. Rev. **75**, 1766–1766 (1949) https://doi.org/10.1103/PhysRev.75.1766.2

[11] Mang, H.J.: Calculation of α-transition probabilities. Phys. Rev. **119**, 1069–1075 (1960) https://doi.org/10.1103/PhysRev.119.1069

[12] Macfarlane, R.D., Siivola, A.: New region of alpha radioactivity. Physical Review Letters **14**(4), 114–115 (1965)

[13] Schardt, D., Kirchner, R., Klepper, O., Reisdorf, W., Roeckl, E., Tidemand-Petersson, P., Ewan, G.T., Hagberg, E., Jonson, B., Mattsson, S., Nyman, G.: Alpha decay studies of tellurium, iodine, xenon and cesium isotopes. Nuclear Physics A **326**(1), 65–82 (1979) https://doi.org/10.1016/0375-9474(79)90367-1

[14] Page, R.D., Woods, P.J., Cunningham, R.A., Davinson, T., Davis, N.J., James, A.N., Livingston, K., Sellin, P.J., Shotter, A.C.: Alpha radioactivity above ^{100}Sn including the decay of ^{108}I. Phys. Rev. C **49**, 3312–3315 (1994) https://doi.org/10.1103/PhysRevC.49.3312

[15] Seweryniak, D., Walters, W.B., Woehr, A., Lipoglavsek, M., Shergur, J., Davids, C.N., Heinz, A., Ressler, J.J.: Population of the 168-kev ($g_{7/2}$) excited state in ^{103}Sn in the α decay of ^{107}Te. Phys. Rev. C **66**, 051307 (2002) https://doi.org/10.1103/PhysRevC.66.051307

[16] Janas, Z., Mazzocchi, C., Batist, L., Blazhev, A., Górska, M., Kavatsyuk, M., Kavatsyuk, O., Kirchner, R., Korgul, A., La Commara, M., Miernik, K.,

Mukha, I., Płochocki, A., Roeckl, E., Schmidt, K.: Measurements of 110xe and 106te decay half-lives. The European Physical Journal A - Hadrons and Nuclei **23**(2), 197–200 (2005)

[17] Liddick, S.N., Grzywacz, R., Mazzocchi, C., Page, R.D., Rykaczewski, K.P., Batchelder, J.C., Bingham, C.R., Darby, I.G., Drafta, G., Goodin, C., Gross, C.J., Hamilton, J.H., Hecht, A.A., Hwang, J.K., Ilyushkin, S., Joss, D.T., Korgul, A., Królas, W., Lagergren, K., Li, K., Tantawy, M.N., Thomson, J., Winger, J.A.: Discovery of ^{109}Xe and ^{105}Te: Superallowed α decay near doubly magic ^{100}Sn. Phys. Rev. Lett. **97**, 082501 (2006) https://doi.org/10.1103/PhysRevLett.97.082501

[18] Auranen, K., Seweryniak, D., Albers, M., Ayangeakaa, A.D., Bottoni, S., Carpenter, M.P., Chiara, C.J., Copp, P., David, H.M., Doherty, D.T., Harker, J., Hoffman, C.R., Janssens, R.V.F., Khoo, T.L., Kuvin, S.A., Lauritsen, T., Lotay, G., Rogers, A.M., Sethi, J., Scholey, C., Talwar, R., Walters, W.B., Woods, P.J., Zhu, S.: Superallowed α decay to doubly magic ^{100}Sn. Phys. Rev. Lett. **121**, 182501 (2018) https://doi.org/10.1103/PhysRevLett.121.182501

[19] Xiao, Y., Go, S., Grzywacz, R., Orlandi, R., Andreyev, A.N., Asai, M., Bentley, M.A., Angelis, G., Gross, C.J., Hausladen, P., Hirose, K., Hofmann, S., Ikezoe, H., Jenkins, D.G., Kindler, B., Léguillon, R., Lommel, B., Makii, H., Mazzocchi, C., Nishio, K., Parkhurst, P., Paulauskas, S.V., Petrache, C.M., Rykaczewski, K.P., Sato, T.K., Smallcombe, J., Toyoshima, A., Tsukada, K., Vaigneur, K., Wadsworth, R.: Search for α decay of ^{104}Te with a novel recoil-decay scintillation detector. Phys. Rev. C **100**, 034315 (2019) https://doi.org/10.1103/PhysRevC.100.034315

[20] Xu, F.R., Pei, J.C.: Mean-field cluster potentials for various cluster decays. Physics Letters B **642**(4), 322–325 (2006) https://doi.org/10.1016/j.physletb.2006.09.048

[21] Xu, C., Ren, Z.: Half lives of α-emitters approaching the $n = z$ line. Phys. Rev. C **74**, 037302 (2006) https://doi.org/10.1103/PhysRevC.74.037302

[22] Mohr, P.: Super-allowed α decay above doubly-magic 100sn and properties of 104te = 100sn $\otimes\alpha$. The European Physical Journal A **31**(1), 23–28 (2007)

[23] Betan, R.I., Nazarewicz, W.: α decay in the complex-energy shell model. Phys. Rev. C **86**, 034338 (2012) https://doi.org/10.1103/PhysRevC.86.034338

[24] Patial, M., Liotta, R.J., Wyss, R.: Microscopic description of superallowed α-decay transitions. Phys. Rev. C **93**, 054326 (2016) https://doi.org/10.1103/PhysRevC.93.054326

[25] Baran, V.V., Delion, D.S.: Proton-neutron versus α-like correlations above ^{100}**Sn**. Phys. Rev. C **94**, 034319 (2016) https://doi.org/10.1103/PhysRevC.94.034319

[26] Yang, S., Xu, C., Röpke, G., Schuck, P., Ren, Z., Funaki, Y., Horiuchi, H., Tohsaki, A., Yamada, T., Zhou, B.: α decay to a doubly magic core in the quartetting wave function approach. Phys. Rev. C **101**, 024316 (2020) https://doi.org/10.1103/PhysRevC.101.024316

[27] Clark, R.M., Macchiavelli, A.O., Crawford, H.L., Fallon, P., Rudolph, D., Såmark-Roth, A., Campbell, C.M., Cromaz, M., Morse, C., Santamaria, C.: Enhancement of α-particle formation near ^{100}Sn. Phys. Rev. C **101**, 034313 (2020) https://doi.org/10.1103/PhysRevC.101.034313

[28] Mercier, F., Zhao, J., Lasseri, R.-D., Ebran, J.-P., Khan, E., Nikšić, T., Vretenar, D.: Microscopic description of the self-conjugate ^{108}Xe and ^{104}Teα-decay chain. Phys. Rev. C **102**, 011301 (2020) https://doi.org/10.1103/PhysRevC.102.011301

[29] Yang, S., Xu, C., Röpke, G.: α-cluster formation and decay: The role of shell structure. Phys. Rev. C **104**, 034302 (2021) https://doi.org/10.1103/PhysRevC.104.034302

[30] Wan, N., Fan, J.: Systematical calculations on α-cluster preformation factors and decay half-lives of light nuclei near the recently observed α emitters ^{108}Xe and ^{104}Te. Phys. Rev. C **104**, 064320 (2021) https://doi.org/10.1103/PhysRevC.104.064320

[31] Wang, Z., Bai, D., Ren, Z.: Improved density-dependent cluster model in α-decay calculations within anisotropic deformation-dependent surface diffuseness. Phys. Rev. C **105**, 024327 (2022) https://doi.org/10.1103/PhysRevC.105.024327

[32] Deng, J.-G., Zhang, H.-F., Sun, X.-D.: New behaviors of α-particle preformation factors near doubly magic 100sn. Chinese Physics C **46**(6), 061001 (2022) https://doi.org/10.1088/1674-1137/ac5a9f

[33] Kubo, T., Kameda, D., Suzuki, H., Fukuda, N., Takeda, H., Yanagisawa, Y., Ohtake, M., Kusaka, K., Yoshida, K., Inabe, N., Ohnishi, T., Yoshida, A., Tanaka, K., Mizoi, Y.: Bigrips separator and zerodegree spectrometer at riken ri beam factory. Progress of Theoretical and Experimental Physics **2012**(1), 03–003 (2012) https://doi.org/10.1093/ptep/pts064 https://academic.oup.com/ptep/article-pdf/2012/1/03C003/11595011/pts064.pdf

[34] Tarasov, O.B., Bazin, D., Hausmann, M., Kuchera, M.P., Ostroumov, P.N., Portillo, M., Sherrill, B.M.,

Tarasova, K.V., Zhang, T.: Lise cute++, the latest generation of the lise ++ package, to simulate rare isotope production with fragment-separators. Nuclear Instruments and Methods in Physics Research Section B: Beam Interactions with Materials and Atoms **541**, 4–7 (2023) https://doi.org/10.1016/j.nimb.2023.04.039

[35] Sümmerer, K., Brüchle, W., Morrissey, D.J., Schädel, M., Szweryn, B., Weifan, Y.: Target fragmentation of au and th by 2.6 gev protons. Phys. Rev. C **42**, 2546–2561 (1990) https://doi.org/10.1103/PhysRevC.42.2546

[36] Sümmerer, K., Blank, B.: Modified empirical parametrization of fragmentation cross sections. Phys. Rev. C **61**, 034607 (2000) https://doi.org/10.1103/PhysRevC.61.034607

[37] Sümmerer, K.: Improved empirical parametrization of fragmentation cross sections. Phys. Rev. C **86**, 014601 (2012) https://doi.org/10.1103/PhysRevC.86.014601

[38] Mei, B.: Improved empirical parameterization for projectile fragmentation cross sections. Phys. Rev. C **95**, 034608 (2017) https://doi.org/10.1103/PhysRevC.95.034608

[39] Ahn, D.S., Amano, J., Baba, H., Fukuda, N., Geissel, H., Inabe, N., Ishikawa, S., Iwasa, N., Komatsubara, T., Kubo, T., Kusaka, K., Morrissey, D.J., Nakamura, T., Ohtake, M., Otsu, H., Sakakibara, T., Sato, H., Sherrill, B.M., Shimizu, Y., Sumikama, T., Suzuki, H., Takeda, H., Tarasov, O.B., Ueno, H., Yanagisawa, Y., Yoshida, K.: Discovery of ^{39}Na. Phys. Rev. Lett. **129**, 212502 (2022) https://doi.org/10.1103/PhysRevLett.129.212502

[40] Tarasov, O.B., Ahn, D.S., Bazin, D., Fukuda, N., Gade, A., Hausmann, M., Inabe, N., Ishikawa, S., Iwasa, N., Kawata, K., Komatsubara, T., Kubo, T., Kusaka, K., Morrissey, D.J., Ohtake, M., Otsu, H., Portillo, M., Sakakibara, T., Sakurai, H., Sato, H., Sherrill, B.M., Shimizu, Y., Stolz, A., Sumikama, T., Suzuki, H., Takeda, H., Thoennessen, M., Ueno, H., Yanagisawa, Y., Yoshida, K.: Discovery of ^{60}Ca and implications for the stability of ^{70}Ca. Phys. Rev. Lett. **121**, 022501 (2018) https://doi.org/10.1103/PhysRevLett.121.022501

[41] Schmidt, K.-H., Sahm, C.-C., Pielenz, K., Clerc, H.G.: Some remarks on the error analysis in the case of poor statistics. Z. Phys. A **316**, 19–26 (1984) https://doi.org/10.1007/BF01415656

[42] Darby, I.G., Grzywacz, R.K., Batchelder, J.C., Bingham, C.R., Cartegni, L., Gross, C.J., Hjorth-Jensen, M., Joss, D.T., Liddick, S.N., Nazarewicz, W., Padgett, S., Page, R.D., Papenbrock, T., Rajabali, M.M., Rotureau, J., Rykaczewski, K.P.: Orbital dependent nucleonic pairing in the lightest known isotopes of tin. Phys. Rev. Lett. **105**, 162502 (2010) https://doi.org/10.1103/PhysRevLett.105.162502

[43] Yokoyama, R., Singh, M., Grzywacz, R., Keeler, A., King, T.T., Agramunt, J., Brewer, N.T., Go, S., Heideman, J., Liu, J., Nishimura, S., Parkhurst, P., Phong, V.H., Rajabali, M.M., Rasco, B.C., Rykaczewski, K.P., Stracener, D.W., Tain, J.L., Tolosa-Delgado, A., Vaigneur, K., WoliÅska-Cichocka, M.: Segmented yso scintillation detectors as a new ion-implant detection tool for decay spectroscopy in fragmentation facilities. Nuclear Instruments and Methods in Physics Research Section A: Accelerators, Spectrometers, Detectors and Associated Equipment **937**, 93–97 (2019) https://doi.org/10.1016/j.nima.2019.05.026

[44] Hamamatsu Photonics: Hamamatsu Photon Is Our Business. https://www.hamamatsu.com/. Accessed: 202341-19 (2024)

[45] Smith, K., Baugher, T., Burcher, S., Carter, A.B., Cizewski, J.A., Chipps, K.A., Febbraro, M., Grzywacz, R., Jones, K.L., Munoz, S., Pain, S.D., Paulauskas, S.V., Ratkiewicz, A., Schmitt, K.T., Thornsberry, C., Toomey, R., Walter, D., Willoughby, H.: First data with the hybrid array of gamma ray detector (hagrid). Nuclear Instruments and Methods in Physics Research Section B: Beam Interactions with Materials and Atoms **414**, 190–194 (2018) https://doi.org/10.1016/j.nimb.2017.06.028

[46] XIA: Pixie-16. https://xia.com/products/pixie-16/. Accessed: 2023-9-21 (2023)

[47] Brun, R., Rademakers, F.: Root - an object oriented data analysis framework. Nucl. Inst. & Meth. in Phys. Res. A, 81–86 (1997) https://doi.org/10.5281/zenodo.848818 . See also "ROOT" software, Release v06.32/02, 18/06/2024

[48] Sun, M.D., Liu, Z., Huang, T.H., Zhang, W.Q., Wang, J.G., Liu, X.Y., Ding, B., Gan, Z.G., Ma, L., Yang, H.B., Zhang, Z.Y., Yu, L., Jiang, J., Wang, K.L., Wang, Y.S., Liu, M.L., Li, Z.H., Li, J., Wang, X., Lu, H.Y., Lin, C.J., Sun, L.J., Ma, N.R., Yuan, C.X., Zuo, W., Xu, H.S., Zhou, X.H., Xiao, G.Q., Qi, C., Zhang, F.S.: New short-lived isotope 223np and the absence of the z?=?92 subshell closure near n?=?126. Physics Letters B **771**, 303–308 (2017) https://doi.org/10.1016/j.physletb.2017.03.074

[49] Mazzocchi, C., Janas, Z., Batist, L., Belleguic, V., Döring, J., Gierlik, M., Kapica, M., Kirchner, R., Lalazissis, G.A., Mahmud, H., Roeckl, E., Ring, P., Schmidt, K., Woods, P.J., ylicz, J.: Alpha decay of 114ba. Physics Letters B **532**(1), 29–36 (2002) https://doi.org/10.1016/S0370-2693(02)01543-5

[50] Capponi, L., Smith, J.F., Ruotsalainen, P., Scholey, C., Rahkila, P., Auranen, K., Bianco, L., Boston,

A.J., Boston, H.C., Cullen, D.M., Derkx, X., Drummond, M.C., Grahn, T., Greenlees, P.T., Grocutt, L., Hadinia, B., Jakobsson, U., Joss, D.T., Julin, R., Juutinen, S., Labiche, M., Leino, M., Leach, K.G., McPeake, C., Mulholland, K.F., Nieminen, P., O'Donnell, D., Paul, E.S., Peura, P., Sandzelius, M., Sarén, J., Saygi, B., Sorri, J., Stolze, S., Thornthwaite, A., Taylor, M.J., Uusitalo, J.: Direct observation of the ^{114}Ba $\rightarrow^{110}$ Xe $\rightarrow^{106}$ Te $\rightarrow^{102}$ Sn triple α-decay chain using position and time correlations. Phys. Rev. C **94**, 024314 (2016) https://doi.org/10.1103/PhysRevC.94.024314

[51] Hinke, C.B., Böhmer, M., Boutachkov, P., Faestermann, T., Geissel, H., Gerl, J., Gernhäuser, R., Górska, M., Gottardo, A., Grawe, H., Gręgosz, J.L., Krücken, R., Kurz, N., Liu, Z., Maier, L., Nowacki, F., Pietri, S., Podolyák, Z., Sieja, K., Steiger, K., Straub, K., Weick, H., Wollersheim, H.-J., Woods, P.J., Al-Dahan, N., Alkhomashi, N., Ataç, A., Blazhev, A., Braun, N.F., Čeliković, I.T., Davinson, T., Dillmann, I., Domingo-Pardo, C., Doornenbal, P.C., France, G., Farrelly, G.F., Farinon, F., Goel, N., Habermann, T.C., Hoischen, R., Janik, R., Karny, M., Kaşkaş, A., Kojouharov, I.M., Kröll, T., Litvinov, Y., Myalski, S., Nebel, F., Nishimura, S., Nociforo, C., Nyberg, J., Parikh, A.R., Procházka, A., Regan, P.H., Rigollet, C., Schaffner, H., Scheidenberger, C., Schwertel, S., Söderström, P.-A., Steer, S.J., Stolz, A., Strmeň, P.: Superallowed Gamow-Teller Decay of the Doubly Magic Nucleus ^{100}Sn. Nature **486**(7403), 341–345 (2012) https://doi.org/10.1038/nature11116

[52] Lubos, D., Park, J., Faestermann, T., Gernhäuser, R., Krücken, R., Lewitowicz, M., Nishimura, S., Sakurai, H., Ahn, D.S., Baba, H., Blank, B., Blazhev, A., Boutachkov, P., Browne, F., Čeliković, I., France, G., Doornenbal, P., Fang, Y., Fukuda, N., Giovinazzo, J., Goel, N., Górska, M., Ilieva, S., Inabe, N., Isobe, T., Jungclaus, A., Kameda, D., Kim, Y.K., Kojouharov, I., Kubo, T., Kurz, N., Kwon, Y.K., Lorusso, G., Moschner, K., Murai, D., Nishizuka, I., Patel, Z., Rajabali, M.M., Rice, S., Schaffner, H., Shimizu, Y., Sinclair, L., Söderström, P.-A., Steiger, K., Sumikama, T., Suzuki, H., Takeda, H., Wang, Z., Warr, N., Watanabe, H., Wu, J., Xu, Z.: Improved value for the gamow-teller strength of the ^{100}Sn beta decay. Phys. Rev. Lett. **122**, 222502 (2019) https://doi.org/10.1103/PhysRevLett.122.222502

[53] Karthein, J., Ricketts, C.M., Garcia Ruiz, R.F., Billowes, J., Binnersley, C.L., Cocolios, T.E., Dobaczewski, J., Farooq-Smith, G.J., Flanagan, K.T., Georgiev, G., Gins, W., Groote, R.P., Gustafsson, F.P., Holt, J.D., Kanellakopoulos, A., Koszorús, Á., Leimbach, D., Lynch, K.M., Miyagi, T., Nazarewicz, W., Neyens, G., Reinhard, P.-G., Sahoo, B.K., Vernon, A.R., Wilkins, S.G., Yang, X.F., Yordanov, D.T.: Electromagnetic properties of indium isotopes illuminate the doubly magic character of 100sn. Nature Physics **20**(11), 1719–1725 (2024)

[54] Wang, Y.Z., Li, Z.Y., Yu, G.L., Hou, Z.Y.: α-decay half-lives around n = z isotopes. Journal of Physics G: Nuclear and Particle Physics **41**(5), 055102 (2014) https://doi.org/10.1088/0954-3899/41/5/055102

[55] Röpke, G., Schnell, A., Schuck, P., Nozières, P.: Four-particle condensate in strongly coupled fermion systems. Phys. Rev. Lett. **80**, 3177–3180 (1998) https://doi.org/10.1103/PhysRevLett.80.3177

[56] Sogo, T., Röpke, G., Schuck, P.: Critical temperature for α-particle condensation in asymmetric nuclear matter. Phys. Rev. C **82**, 034322 (2010) https://doi.org/10.1103/PhysRevC.82.034322

[57] Xu, C., Ren, Z., Röpke, G., Schuck, P., Funaki, Y., Horiuchi, H., Tohsaki, A., Yamada, T., Zhou, B.: α-decay width of ^{212}Po from a quartetting wave function approach. Phys. Rev. C **93**, 011306 (2016) https://doi.org/10.1103/PhysRevC.93.011306

[58] Schuck, P., Funaki, Y., Horiuchi, H., Röpke, G., Tohsaki, A., Yamada, T.: Quartetting in fermionic matter and α-particle condensation in nuclear systems. Progress in Particle and Nuclear Physics **59**(1), 285–304 (2007) https://doi.org/10.1016/j.ppnp.2006.12.003 . International Workshop on Nuclear Physics 28th Course

[59] Funaki, Y., Horiuchi, H., Oertzen, W., Röpke, G., Schuck, P., Tohsaki, A., Yamada, T.: Concepts of nuclear α-particle condensation. Phys. Rev. C **80**, 064326 (2009) https://doi.org/10.1103/PhysRevC.80.064326

[60] Röpke, G., Schuck, P., Funaki, Y., Horiuchi, H., Ren, Z., Tohsaki, A., Xu, C., Yamada, T., Zhou, B.: Alpha decay width of 212po from a quartetting wave function approach. Journal of Physics: Conference Series **863**(1), 012006 (2017) https://doi.org/10.1088/1742-6596/863/1/012006

[61] Typel, S., Röpke, G., Klähn, T., Blaschke, D., Wolter, H.H.: Composition and thermodynamics of nuclear matter with light clusters. Phys. Rev. C **81**, 015803 (2010) https://doi.org/10.1103/PhysRevC.81.015803

[62] Henzlova, D., Schmidt, K.-H., Ricciardi, M.V., ć, A., Henzl, V., Napolitani, P., Audouin, L., Benlliure, J., Boudard, A., Casarejos, E., Ducret, J.E., Enqvist, T., Heinz, A., Junghans, A., Jurado, B., Krása, A., Kurtukian, T., Leray, S., Ordóñez, M.F., Pereira, J., č, R., Rejmund, F., Schmitt, C., Stéphan, C., Tassan-Got, L., Villagrasa, C., Volant, C., Wagner, A., Yordanov, O.: Experimental investigation of the residues produced in the ^{136}Xe + Pb and ^{124}Xe + Pb

fragmentation reactions at 1a gev. Phys. Rev. C **78**, 044616 (2008) https://doi.org/10.1103/PhysRevC.78.044616

[63] Suzuki, H., Kubo, T., Fukuda, N., Inabe, N., Kameda, D., Takeda, H., Yoshida, K., Kusaka, K., Yanagisawa, Y., Ohtake, M., Sato, H., Shimizu, Y., Baba, H., Kurokawa, M., Ohnishi, T., Tanaka, K., Tarasov, O.B., Bazin, D., Morrissey, D.J., Sherrill, B.M., Ieki, K., Murai, D., Iwasa, N., Chiba, A., Ohkoda, Y., Ideguchi, E., Go, S., Yokoyama, R., Fujii, T., Nishimura, D., Nishibata, H., Momota, S., Lewitowicz, M., DeFrance, G., Celikovic, I., Steiger, K.: Production cross section measurements of radioactive isotopes by bigrips separator at riken ri beam factory. Nuclear Instruments and Methods in Physics Research Section B: Beam Interactions with Materials and Atoms **317**, 756–768 (2013) https://doi.org/10.1016/j.nimb.2013.08.049 . XVIth International Conference on ElectroMagnetic Isotope Separators and Techniques Related to their Applications, December 2–7, 2012 at Matsue, Japan

[64] Vertilon: Position Sensitive PMT Interface Products. Date Accessed = August 27, 2025. https://vertilon.com/products_sensor/